Supporting information

One stone, two birds: robust and self-absorption free flexible perovskite scintillators by metal organic frameworks encapsulation

Jie zhou[a,b], Zhouyuanhang Wang[a,b], Zhongren Shi[b], Xilin Zhang[a,b], Lan Yang[a,b], Yuxuan Jiang[a,c], Yan Kuai[b], Zhijia Hu*[a,b], Siqi Li*[a,b]

a. School of Physics and Optoelectronic Engineering, Key Laboratory of Opto-Electronic Information Acquisition and Manipulation of Ministry of Education, Anhui University, Hefei, 230601, Anhui, P. R. China.

b. Information Materials and Intelligent Sensing Laboratory of Anhui Province, Anhui University, Hefei, 230601, Anhui, P. R. China.

c. Center of Free Electron Laser & High Magnetic Field, Anhui University, Hefei, 230601, Anhui, P. R. China

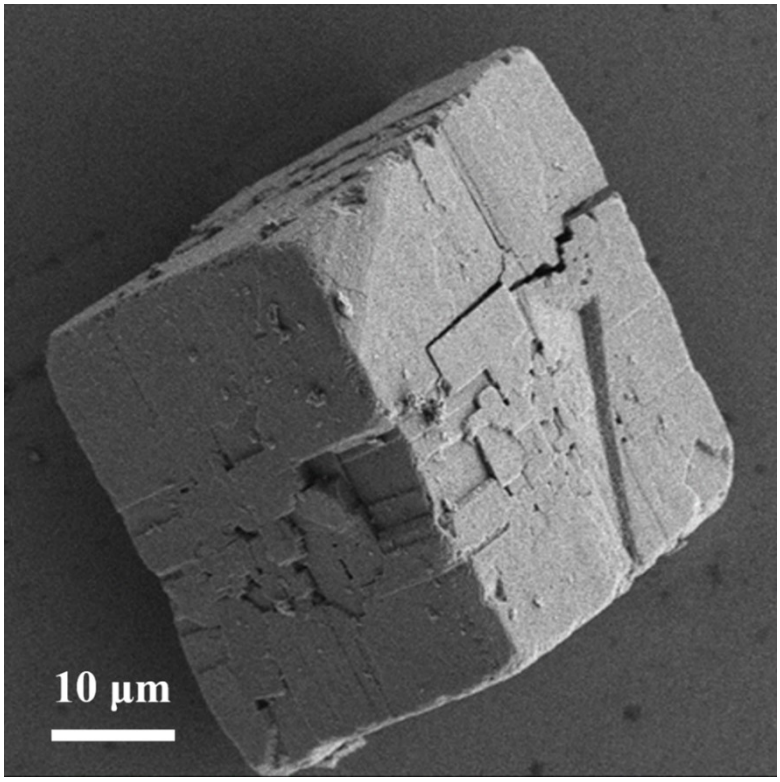

Figure S1: SEM image of MOF-5 crystals.

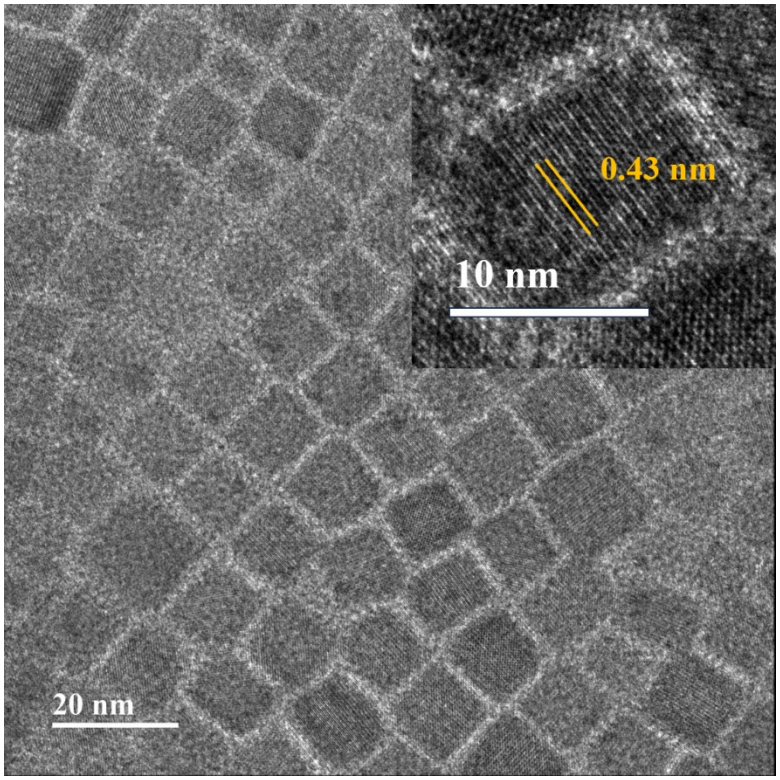

Figure S2: TEM image of $CsPbBr_3$ NCs with a scale bar of 20 nm. Inset: high-resolution TEM image of $CsPbBr_3$ NCs with a scale bar of 10 nm.

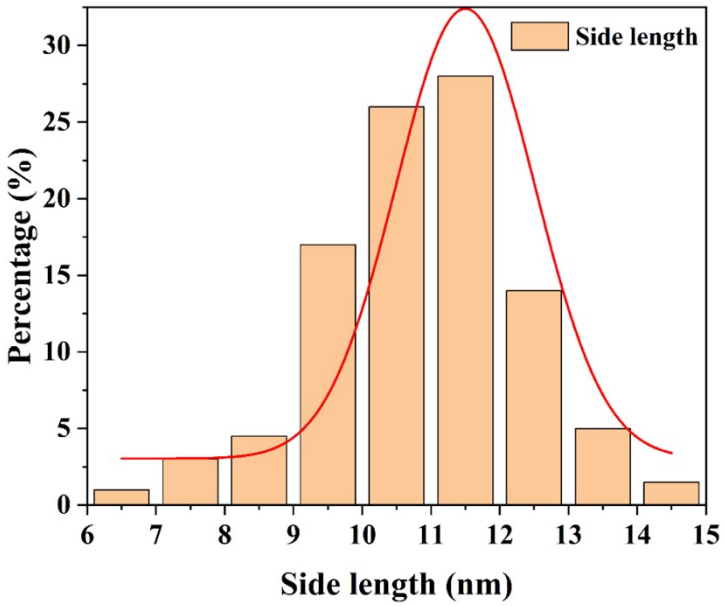

Figure S3: Particle size distribution of $CsPbBr_3$ NCs.

Table S1: BET specific surface area, specific pore volume, and average pore size of MOF-5 and $CsPbBr_3$/MOF-5.

sample	S_{BET} (m^2/g)	Pore volume (cm^3/g)	Average pore size (nm)
MOF-5	598.8	0.3470	5.052
$CsPbBr_3$/MOF-5	377.4	0.2370	6.928

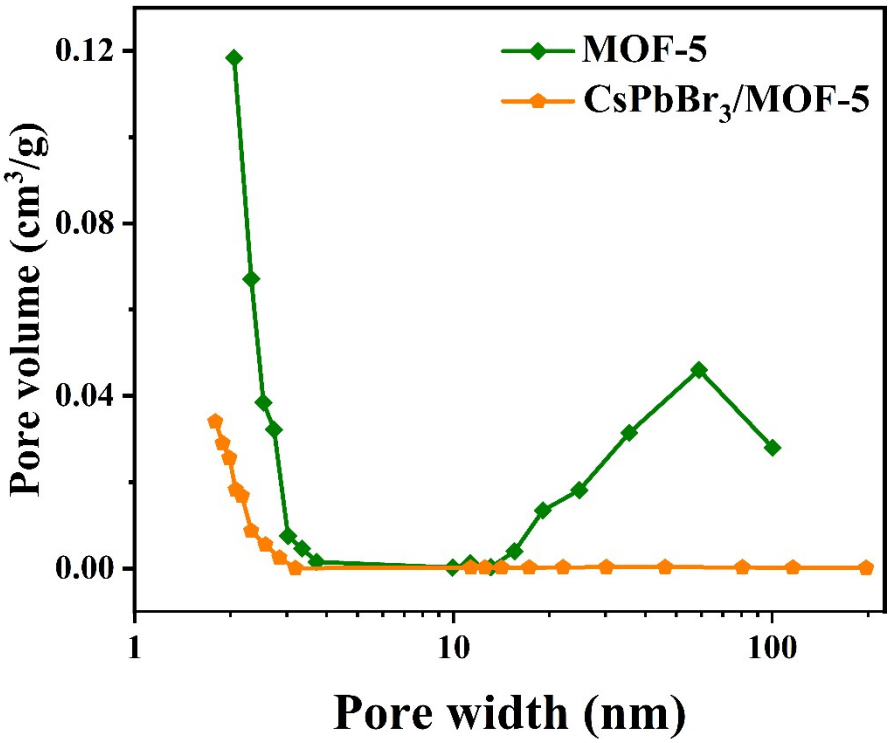

Figure S4: Pore diameter distributions of the MOF-5 and $CsPbBr_3$/MOF-5 samples.

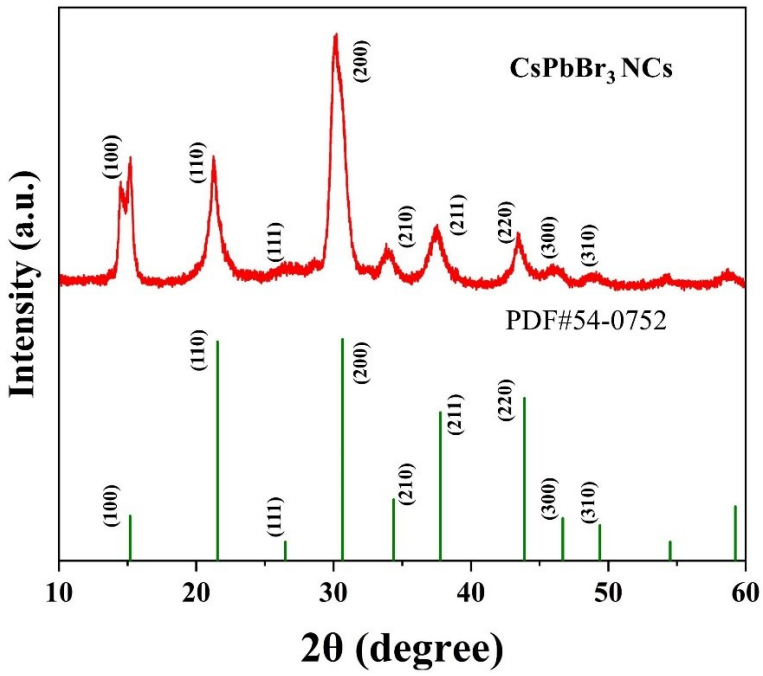

Figure S5: XRD pattern of $CsPbBr_3$ NCs with the PDF#54-0752.

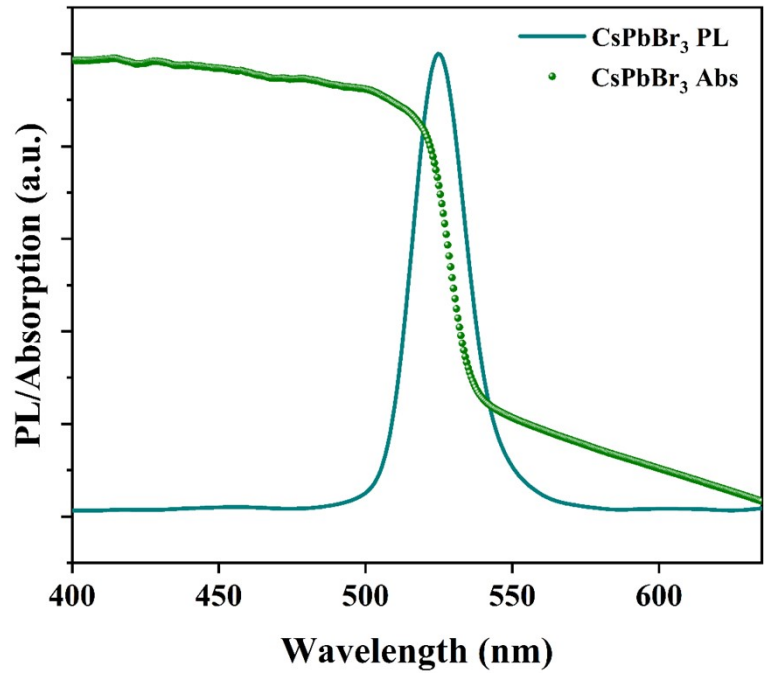

Figure S6: UV-Vis absorption and PL spectra of $CsPbBr_3$ NCs.

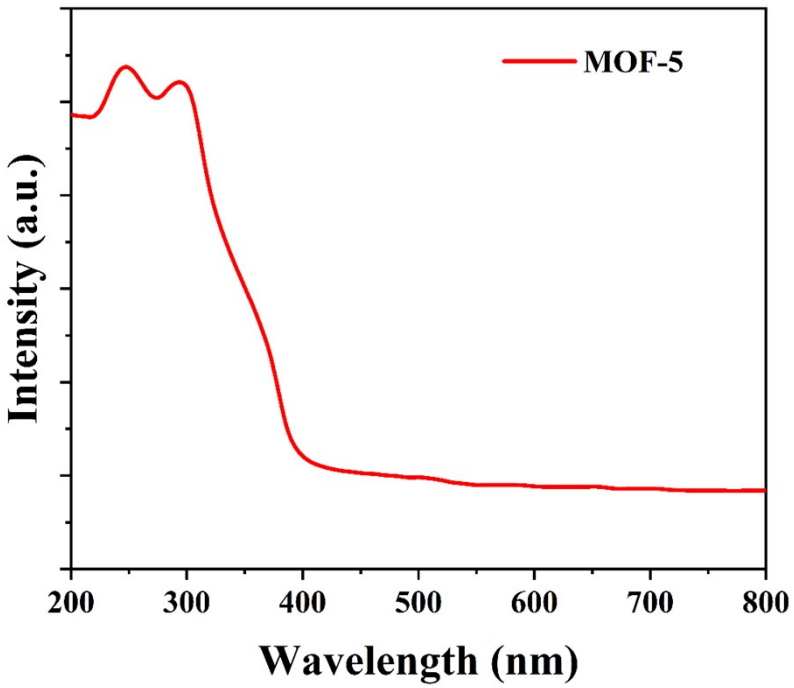

Figure S7: UV-Vis absorption diagram of pure MOF-5.

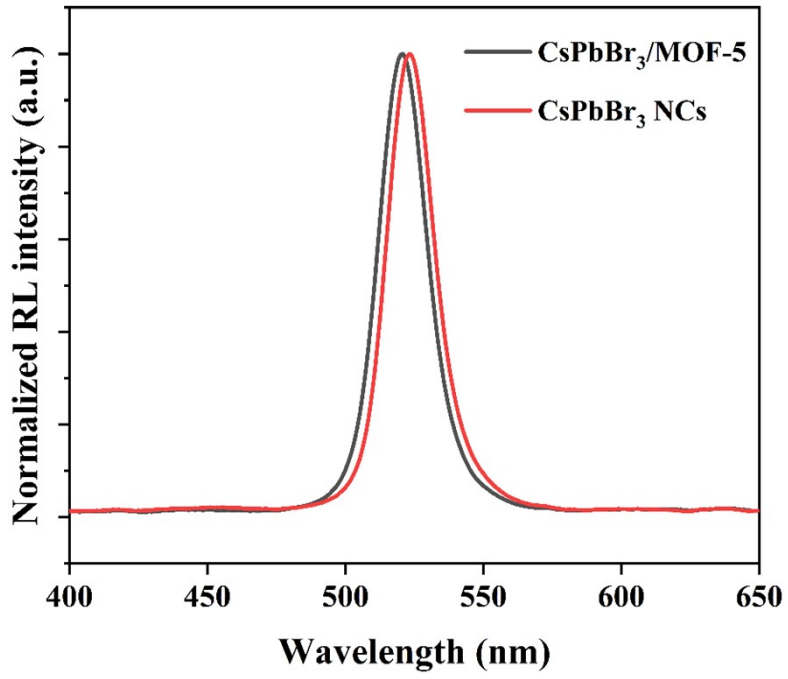

Figure S8: RL spectra of $CsPbBr_3$ NCs and $CsPbBr_3$/MOF-5 composite film.

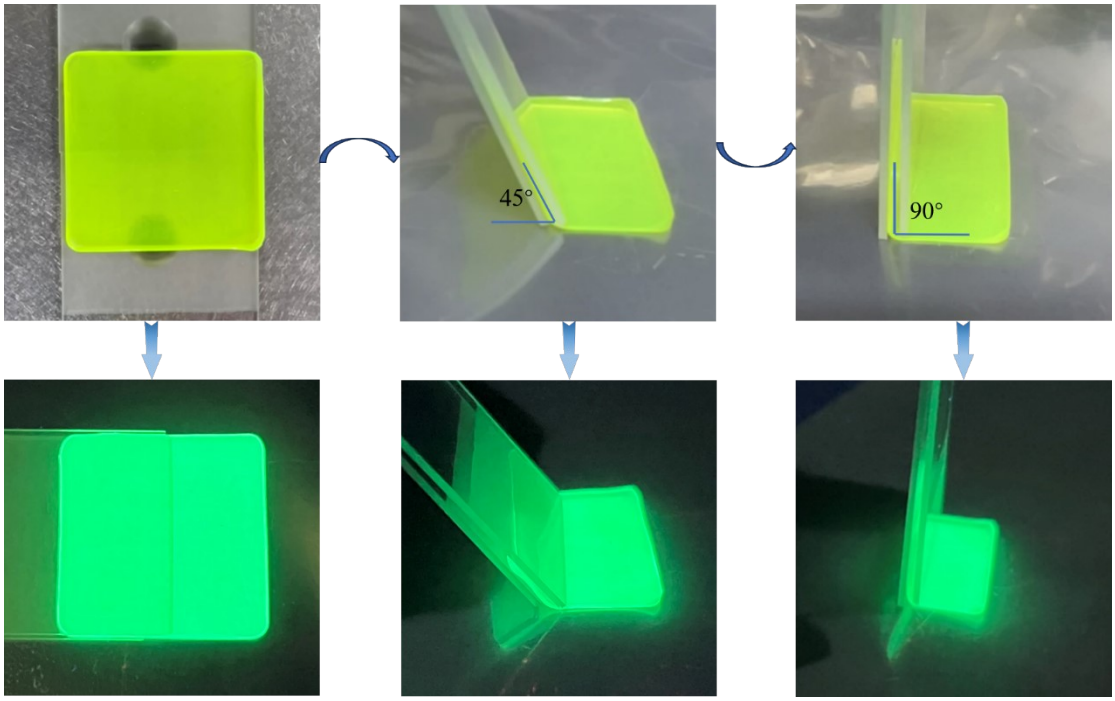

Figure S9: Bending test of $CsPbBr_3$/MOF-5 composite film with different degrees.

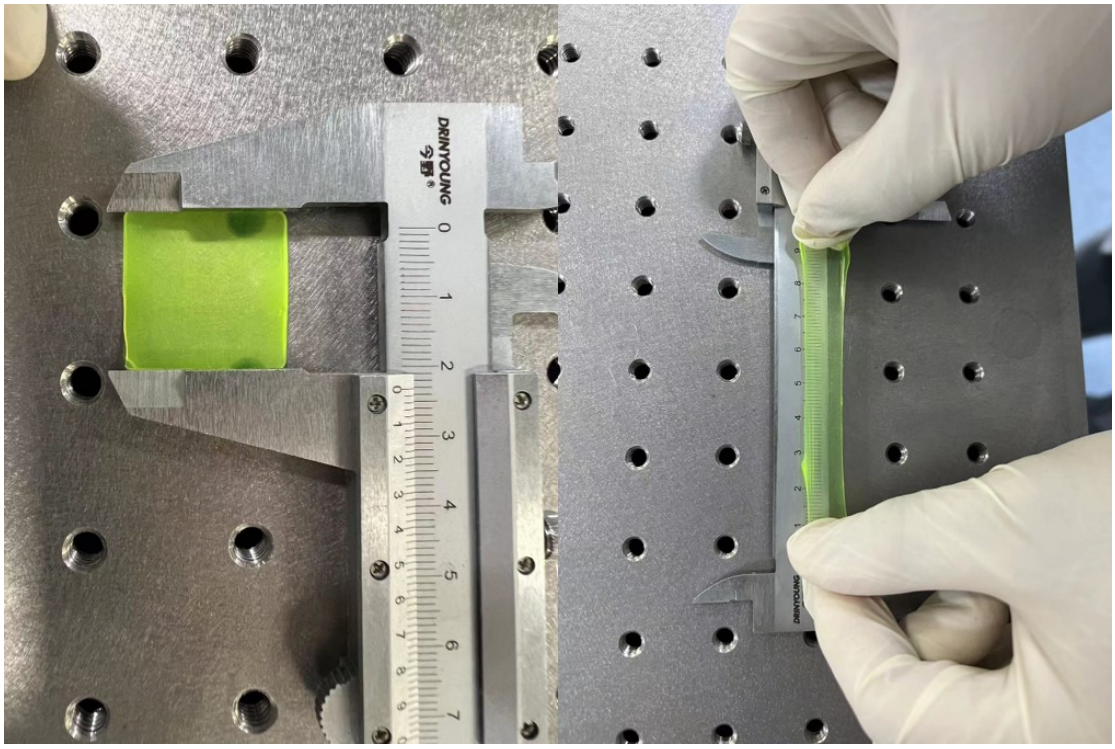

Figure S10: Stretching of $CsPbBr_3$/MOF-5 composite film to 5 times its original length.

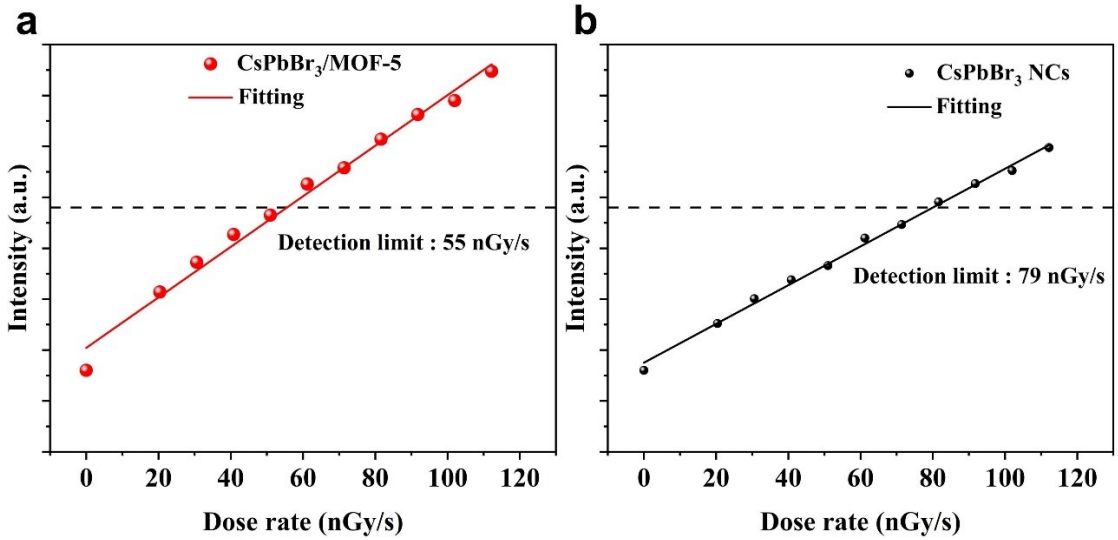

Figure S11: The detection limits of $CsPbBr_3$/MOF-5 composite film(a) and $CsPbBr_3$ NCs film(b) were determined after 1-hour radiation at a dose rate of 2 mGy/s.

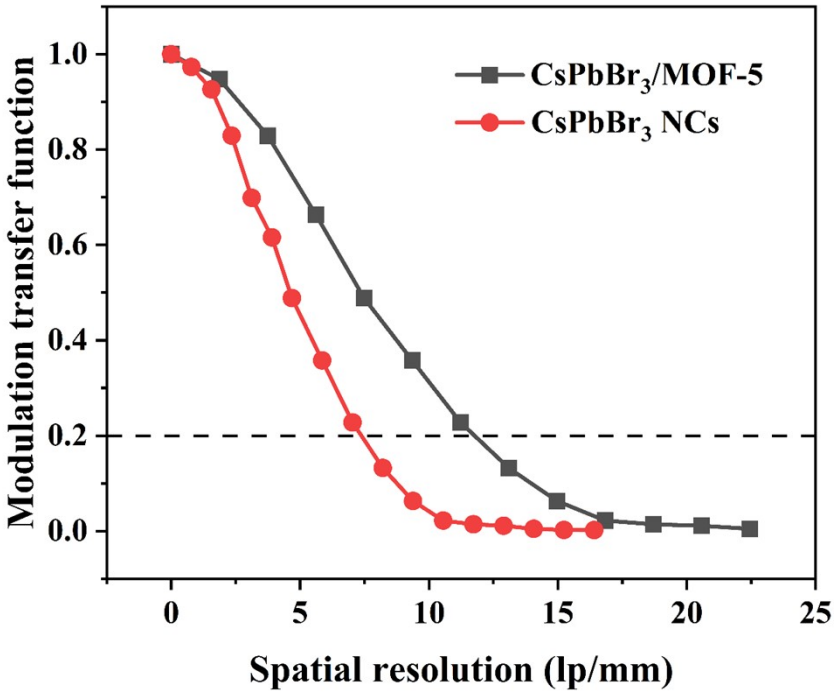

Figure S12: The resolution of $CsPbBr_3$/MOF-5 composite film and $CsPbBr_3$ film were evaluated after 1-hour radiation at a dose rate of 2 mGy/s.

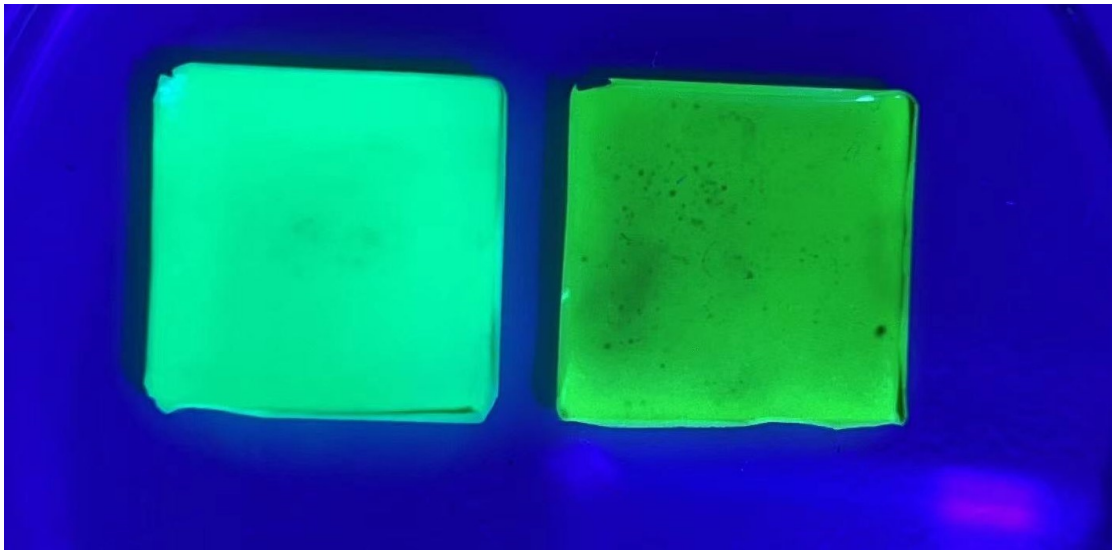

Figure S13: The $CsPbBr_3$/MOF-5 composite film (left) and the $CsPbBr_3$ NCs film (right) were stored under the same conditions for 120 days. Significant damage to the $CsPbBr_3$ NCs film could be seen under 365 nm UV light.

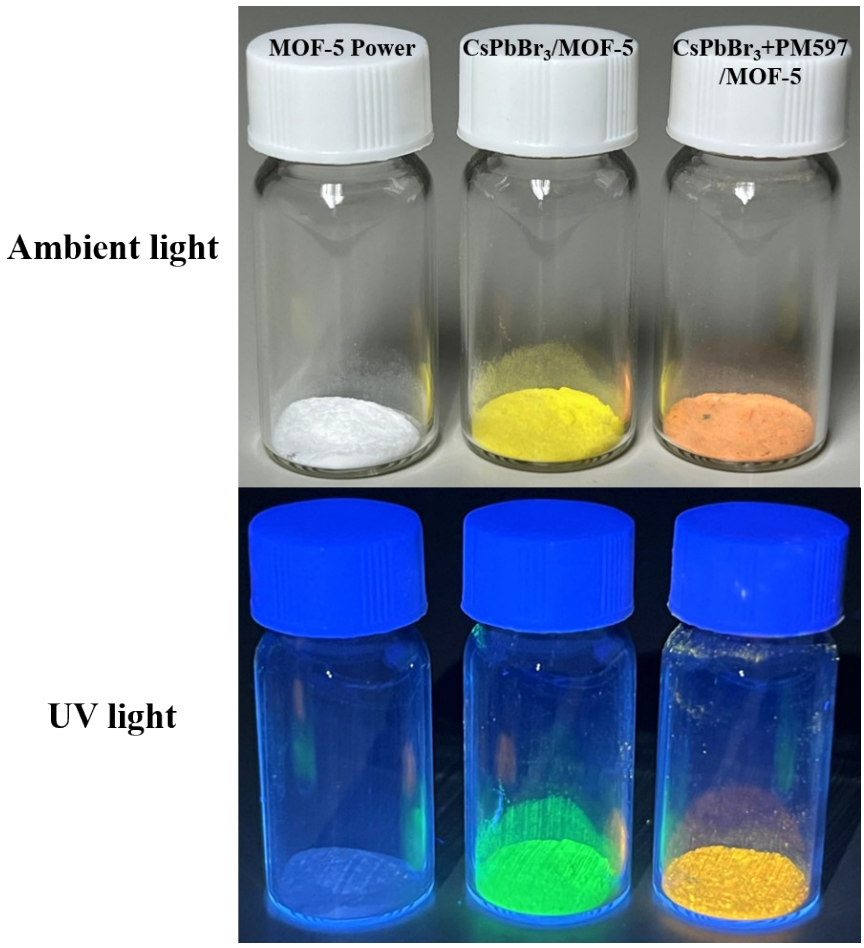

Figure S14: MOF-5 powder, $CsPbBr_3$/MOF-5 powder, and $CsPbBr_3$+PM597/MOF-5 powder under ambient light and UV light.

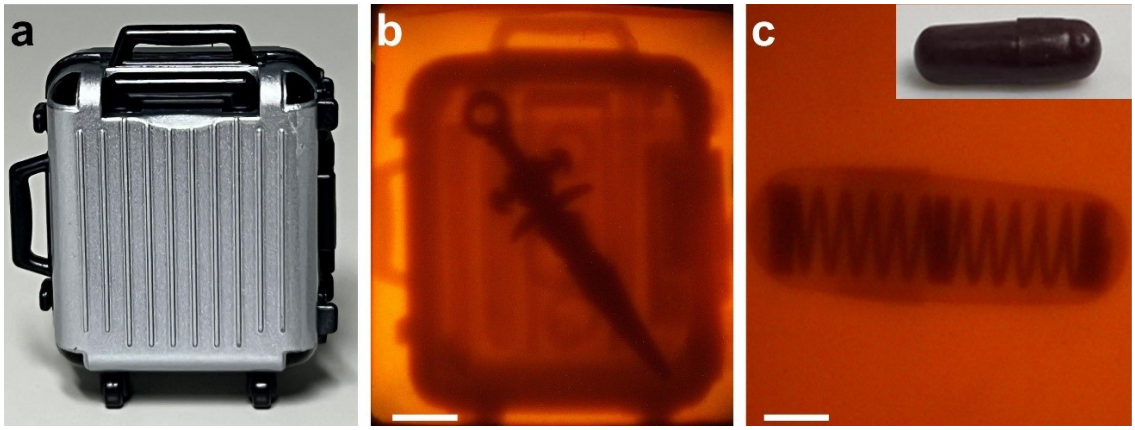

Figure S15: (a-b) Photographs of a miniature traveling case (containing a metal sword) and photographs of its X-ray image, scale bar is 1 cm. (c) Capsule (containing a spring) photographed through $CsPbBr_3$+PM597/MOF-5 composite film and photographs of its X-ray image, scale bar is 3 mm.

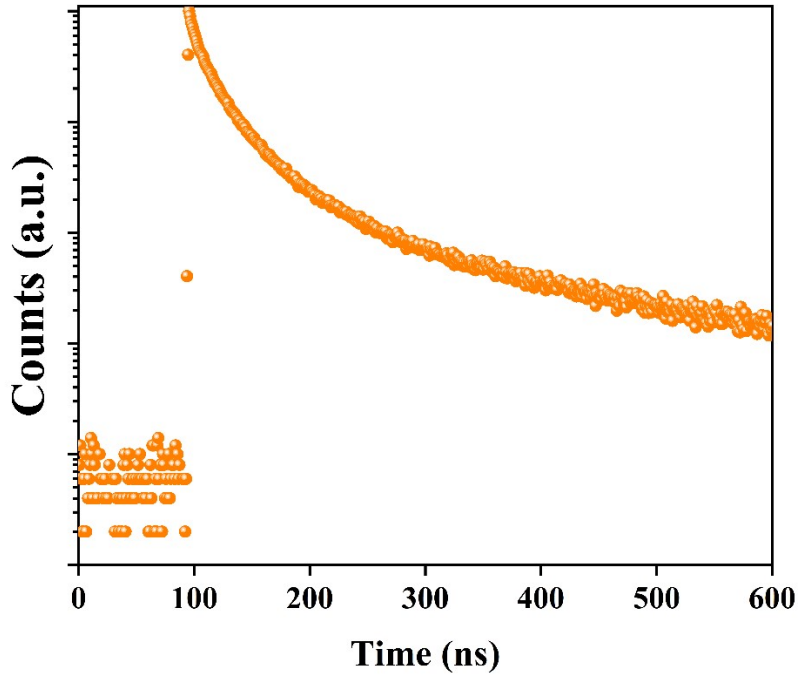

Figure S16: Photoluminescence decay curves of $CsPbBr_3$/MOF-5 composites at the center wavelength under laser excitation at 373 nm.

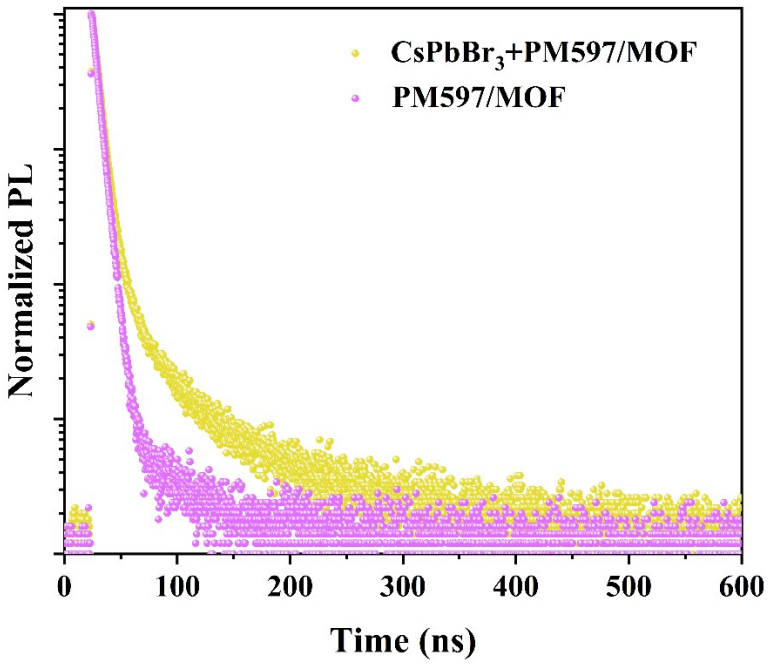

Figure S17: Photoluminescence decay curves of $CsPbBr_3$+PM597/MOF and PM597/MOF.

Table S2. Fitting parameters of $CsPbBr_3$/MOF, $CsPbBr_3$+PM597/MOF, and PM597.

Sample	τ_1 (ns)	τ_2 (ns)	A_1	A_2	τ_{avg} (ns)
$CsPbBr_3$/MOF	70	12.9	0.89	0.11	35.78
$CsPbBr_3$+PM597/MOF	53	5.3	0.015	0.985	11.58
PM597/MOF	5.32	5.32	0.003	0.997	5.32

Photoluminescence quantum yield (PLQY)

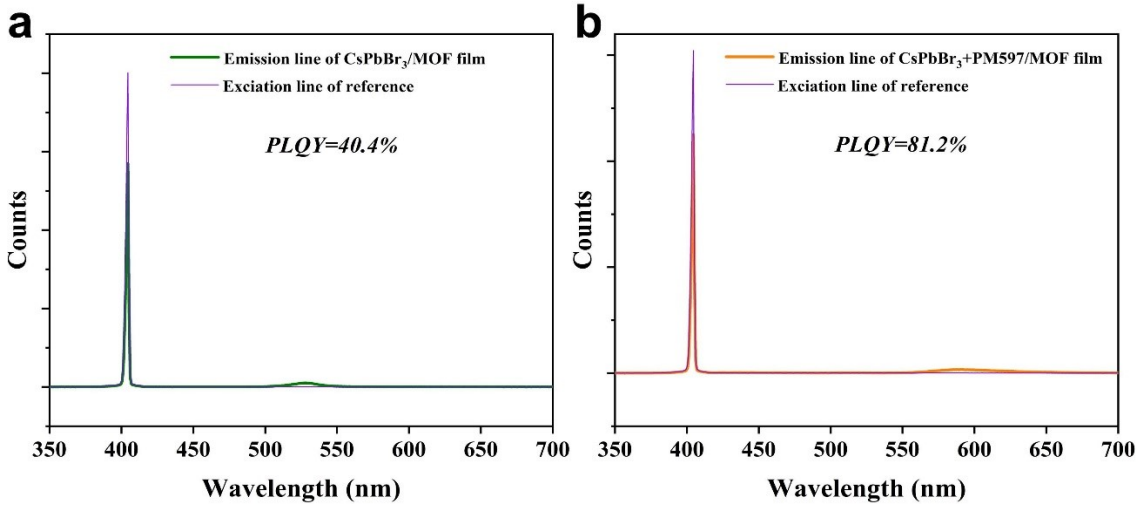

Figure S18: The PLQY of $CsPbBr_3$/MOF-5 film and $CsPbBr_3$+PM597/MOF-5 film.

We measured the PLQY of $CsPbBr_3$/MOF-5 film and $CsPbBr_3$+PM597/MOF-5 film using an integrating sphere as shown in Table S3. PLQY is defined as the ratio of photon numbers emitted to the number of photons absorbed[1, 2]:

$$PLQY = \frac{n\ (photons\ emitted)}{n\ (photons\ absorbed)} * 100\%\#(1)$$

Table S3. Comparison of the PLQY for different samples

Sample	Integration area of absorption (math.)	Integration area of emission (math.)	PLQY(%)
$CsPbBr_3$ /MOF film	15838	6393	40.4
$CsPbBr_3$+PM597/MOF film	12138	9853	81.2

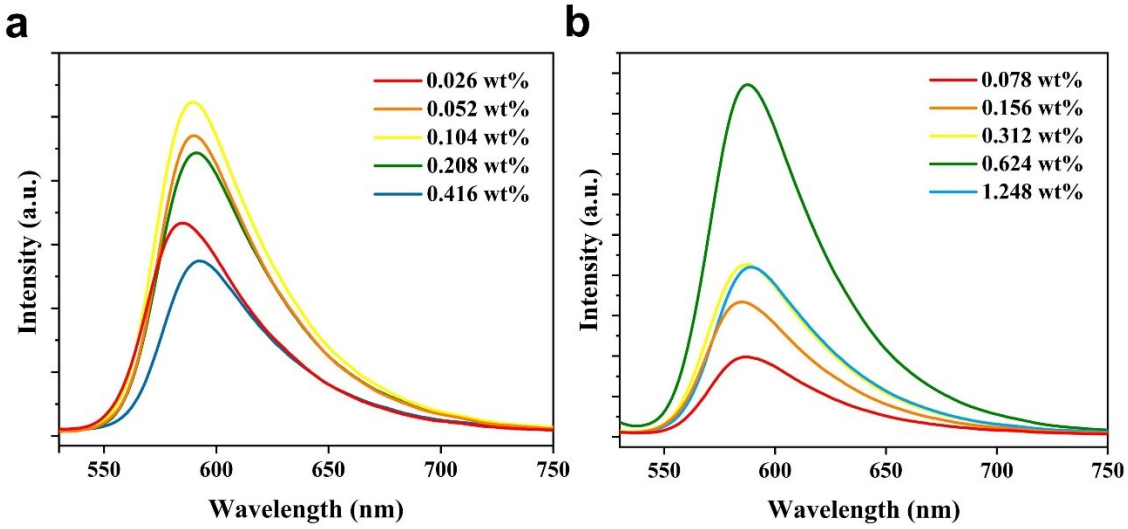

Figure S19: (a) RL spectra evolution of $CsPbBr_3$ +PM597 solid films under X-ray with PM597 concentration from 0.026 to 0.416 wt%; (b) RL spectra evolution of $CsPbBr_3$ +PM597/MOF-5 solid films under X-ray with PM597 concentration from 0.078 to 1.248 wt%.

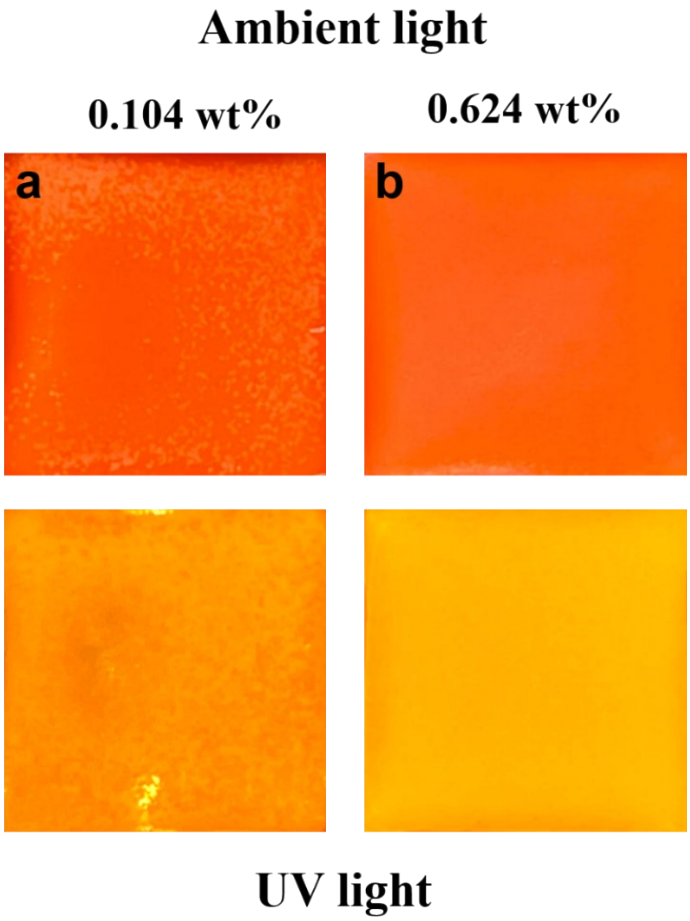

Figure S20: Comparison of physical images of $CsPbBr_3$+PM597 and $CsPbBr_3$+PM597/MOF-5 films. Sample a is a $CsPbBr_3$+PM597 film with a PM597 concentration of 0.104 wt%, while sample b is a $CsPbBr_3$+PM597/MOF-5 film with a PM597 concentration of 0.624 wt%. The upper images were captured under ambient light, and the lower images were taken under UV light (365 nm).

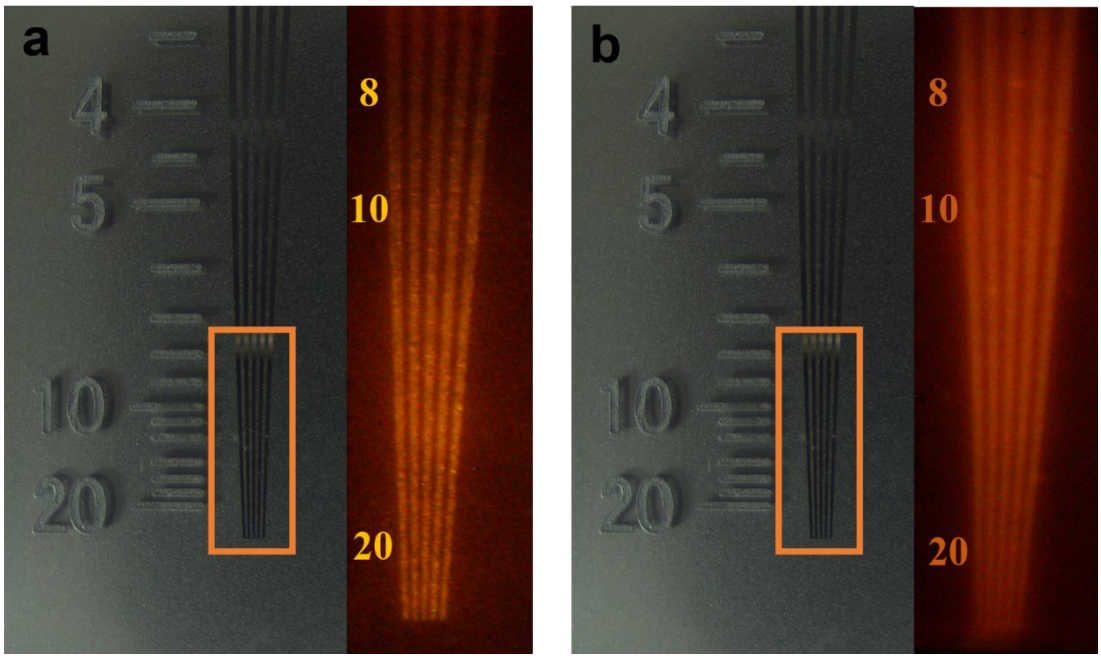

Figure S21: The standard X-ray test-pattern plate imaging of (a) $CsPbBr_3$+PM597/MOF-5 composite film and (b) $CsPbBr_3$+PM597 composite film.

References

1. J.-X. Wang, O. Shekhah, O. M. Bakr, M. Eddaoudi and O. F. Mohammed, *Chem.*, 2024.
2. S. Tian, Z. Shi, Y. Sun, P. Zhang, S. Wu, D. Chen, P. Xiong, Q. Qian and Z. Yang, *Laser Photonics Rev.*, 2022, **16**, 2200020.